FEASIBILITY STUDY OF SURROGATE MODEL FOR THE APPLICATION OF VEHICLE SUSPENSION SYSTEM

A. Dzakaria*, S. Mansor, S.A.A Bakar

School of Mechanical Engineering,
Universiti Teknologi Malaysia,
81310 UTM Skudai, Johor.

Article history
Received
21st July 2021
Received in revised form
8th August 2021
Accepted
10th September 2021
Published
12th September 2021

*Corresponding author
dafandi@mail.fkm.utm.my

GRAPHICAL ABSTRACT

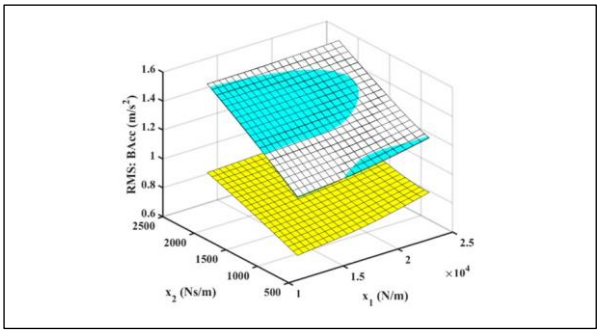

ABSTRACT

High-fidelity (HF) model always provides better performance in assessing vehicle suspension system design compared to low-fidelity (LF) model. However, HF model is computationally expensive. On the contrary, LF model, which depends on a few parameters allow the simulation of 'what-if' problem run faster and the results potentially comparable with HF model. This research attempts to conduct feasibility study on LF model using surrogate model for the application of vehicle suspension study. The surrogate models are classified into three types which are Response-Based (RB) model, Variable-Based (VB) model, and Parameter-Based (PB) model. Through three statistical metrics and graphical interpretation, the results show that VB model gave the most superior performance compared to RB model and PB model.

KEYWORDS

Low-fidelity model; high-fidelity model; surrogate model

INTRODUCTION

Over the last two decades, the design of passive vehicle suspension system is greatly based on running the predictive model for the computer experiments. The term predictive model refers to a mathematical model that represent a system by mathematical relations [1]. With good predictive model, the effect of new component toward existing subsystems can be analysed long before the prototype is built [2].

Rapid progress in computer technology had caused attraction to increase the complexity to the predictive model. The main objective of the effort is to digitize the real physical behaviour and provide a useful tool w but, most importantly, to adjust parameters of the system so that it meets the performance target requirements [3]. However, the simulation of such model is computationally expensive and time consuming since it requires more data and funding to fulfil it [4]. On the other hand, the model is also expected to have the simplest representation to allow efficient and fast simulations of the vehicle dynamics for improving the efficiency of the total engineering design process. An oversimplified model will not be capable of revealing important effects. These conflicting requirements show that modelling is a challenging design task, in particular, for

complex systems like suspension system. Sharp [5] said that

> "*The ideal model is that minimum complexity which is capable of solving the problems of concern with an acceptable risk of the solution being 'wrong'. This acceptable risk is not quantifiable and it must remain a matter of judgement*".

[6], [7], [8], [3], and [9] have proposed the potentiality solution for these conflicting requirements is by implementing a surrogate model. The surrogate model will later substitute the role of the high-fidelity model in the further engineering design tasks. This strategy will speed up the design process and potentially become a compulsory tool in modern concurrent engineering practice.

The subject of passive suspension system modeling and surrogate modeling are abundantly available in the literature. However, the number of published literatures that integrate vehicle suspension system model and surrogate model are still in small amounts.

There are two formulation approaches for the ride and handling models architecture which are called as lumped mass approach and multi-body system approach. The algebraic-differential lumped mass model is normally used in the modeling and simulation of suspension system during the early car design phase. All the car parts are decomposed into three elementary elements, i.e., inertia, damping, and stiffness. Then, appropriate linking is configured to connect these elements and forming a single or multiple degrees-of-freedom car model. In general, there are numerous degrees-of-freedom associated with this type of model. The number of degrees-of-freedom (dof) of the model is vary from one simulation to another depending on the level details required. A free-floating rigid body in three-dimensional space has six dof, i.e., three translational freedoms and three rotational freedoms which respect to the *x*, *y*, and *z* axes respectively. Figure 1(a) shows the most basic ride model, one dof of quarter car model. All the car's masses are lumped together as one unit and the tire is assumed as a rigid body. Quarter car model (QCM) is a single station of suspension system or one fourth of the vehicle. This model is mostly used to teach undergraduate student about the fundamental concept of vibration and gaining general understanding of the system. [10] used 1 dof model to develop basic understanding of skyhook algorithms on the active and semi-active suspension systems and then optimize it by using an evolutionary algorithm. However, this model is inadequate for ride study [11]. Most of researchers in vehicle dynamics agree that the suspension system acts as a mediator between unsprung body and sprung body. In order to capture these masses behavior, the researchers increase the dof from one to two. In 2 dof, there are two masses where each mass represents the unsprung mass and sprung mass respectively (Figure 1(b)). This model is known as the lowest fidelity model to study ride dynamics behaviour [12], receive the largest attention in the literature, and has capability to capture a pure heave dynamics behavior only.

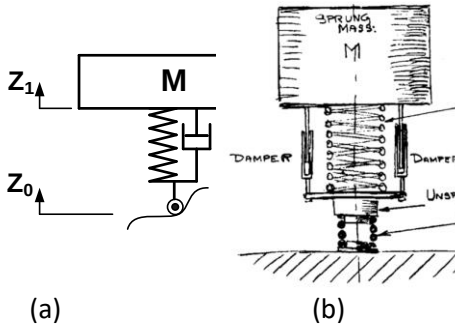

Figure 1: (a) one dof model and (b) two dof model (was sketched by [12]).

Increasing the dof number to 4 dof allows the behavior of bounce-and-rolling dynamics, and bounce-and-pitching dynamics to be studied. The 4 dof model is also known as half car model (HCM). If the layout of HCM is in a lateral plane, it is intended for bounce-and-rolling dynamics simulation [13]. Moreover, the bounce-and-pitching dynamics simulation requires the HCM's layout to be in longitudinal plane [14]. However, QCM and HCM do not have enough complexity to be used for interpreting the combining effect of bounce, rolling, and pitching motions. To satisfy this complex necessity, the dof number is increased to 7 dof. Seven dof system model is a three-dimensional

model, and can representing a full car model (FCM). [15] refer this 7 dof as reduced-order model compared to MBS full car model. The reduced-order model is linearized FCM can be used to predict the sprung roll motion, sprung pitch motion, sprung bounce motion, and four corners unsprung bounce motion performances [16]. [17] shows have added anti-roll bar effect into 7 dof system model. However, this effect can be ignored for studying a normal road ride [4]. On the other research, due to center height of gravity, and roll center of military truck is considered high, [17] again take the roll axis effect into account of ride dynamics performance. Both effects provide better accuracy in aspect of rolling response prediction, even though the dof does not increases. However, the inclusion of [18] has developed 14 dof model with 6 dof of sprung body and 2 dof at each of four corners to simulate vehicle rollover. Ghike's 14 dof model has included roll center in the derivation, capable to calculate vertical body response at each sprung body corner compared to 7 dof model, and the model validation is carried out against the responses produced by two standard softwares, i.e., CarSim and MSC Adams model. They have claimed that 14 dof is able to produce more detailed prediction. [19] has derived and validated 16 dof of lumped mass model. The integration of 7 dof of ride model and 9 dof of handling model created the 16 dof model. This 16 dof model allows to simulate ride and handling characteristics simultaneously. However, this research has chosen 7 dof model to be as the high-fidelity model due to this model has been recognized as adequate to representing full car's ride characteristics.

Based on the literature review done to the date of this paper submission, it was impossible to enhance the quality of quarter car model's responses (which in this case is low-fidelity model) so that it will match to the quality of full car model's responses (which in this case is high-fidelity model) if the surrogate model formulation depends purely based on the physics principles. The integration between global approximation model and physic-based surrogate model were found having potential to formulate one variant of surrogate model for vehicle suspension application. The key role of this new variant of surrogate model is to replace the usage of high-fidelity model in later works such as optimizing the suspension setting. In order to establish this paper's research, three global approximation modeling methods, which had received great attention recently are reviewed. The methods are Polynomial Model, Radial Basis Function Model, and Kriging Model.

Polynomial Model. Taylor's theorem states that any smooth function can be approximated by infinite series of polynomial terms [20]. Taylor series expansion then provides a mechanism to express this idea for producing useful results [1]. Eq. 1 shows one-dimensional expression of this series expansion, where $f^{(n)}(x_i)$ is the nth derivative at x_i, and x_i is a current or reference point.

$$F(x_{i+1}) = \sum_{n=0}^{\infty} \frac{F^{(n)}(x_i)}{n!}(x_{i+1} - x_i)^n \quad (1)$$

Due the infinite series (Eq. 1) is difficult to be handled in common practice, infinity term is separated into some first N terms and a remainder R_N as written in Eq. 2 [1]. Equation 3 is an approximation function after R_N term is neglected because of small in value. This equation is very useful in doing local approximation.

$$F(x_{i+1}) = \sum_{n=0}^{N} \frac{F^{(n)}(x_i)}{n!}(x_{i+1} - x_i)^n + R_N \quad (2)$$

$$F(x_{i+1}) = \sum_{n=0}^{N} \frac{F^{(n)}(x_i)}{n!}(x_{i+1} - x_i)^n \quad (3)$$

The only unknowns in Eq. 4 re the values at the prediction x_{i+1}. Then, [20] recomposed this equation and stated as

$$F(h) = \alpha_0 + \alpha_1 h + \alpha_2 h^2 + \cdots + \alpha_n h^n \quad (4)$$

The flexure property owned by Eq. 5 make it turn into the most dominant expression of polynomial function and widely rewritten as

$$F(x) = a_0 + a_1 x + a_2 x^2 + \cdots + a_n x^n \quad (5)$$

The coefficients of a_0, a_1, a_2, …, a_n are real numbers ($\mathbb{R}$), and n is a non-negative integer, is the degree or order of the polynomial. A first-order polynomial is a linear function, and higher-order polynomials are so-called non-linear functions [21]. A more generic polynomial model is mathematically written as

$$F(z) = w_0 z_0 + w_1 z_1 + \cdots + w_m z_m + \varepsilon, \quad (6)$$

where $z_0, z_1, \ldots, z_m$ are $m + 1$ basis functions, and ε is the error. Eq. 7 can also be expressed in matrix form as

$$\{F(\boldsymbol{z})\} = [\boldsymbol{\zeta}]\{\boldsymbol{w}\} + \{\boldsymbol{\varepsilon}\} \quad (7)$$

where $\boldsymbol{\zeta}$ is the Vandermonde matrix (i.e., Eq. 8).

$$\zeta = \begin{bmatrix} z_{01} & z_{11} & z_{21} & \cdots & z_{m1} \\ z_{02} & z_{12} & z_{22} & \cdots & z_{m2} \\ \vdots & \vdots & \vdots & \vdots & \vdots \\ z_{0n} & z_{1n} & z_{2n} & \cdots & z_{mn} \end{bmatrix} \quad (8)$$

The maximum likelihood estimates of $\boldsymbol{w}$ are unknown tuning factors and is satisfied through minimizing the sum the squares of the errors ε.

$$\boldsymbol{w} = \boldsymbol{\zeta}^{+} F(\boldsymbol{z}) \quad (9)$$

where $\boldsymbol{\zeta}^{+} = (\boldsymbol{\zeta}^T \boldsymbol{\zeta})^{-1} \boldsymbol{\zeta}^T$ is the Moose-Penrose pseudo-inverse of $\boldsymbol{\zeta}$. [22] and [23] have recomposed this method and called this model as mechanistic model. They have utilized this mechanistic model in structural optimization problem

Radial Basis Function Model. Hardy in 1971 was the first proposed the idea of using Radial Basis Function Model (RBFM) as approximation function [24].

RBFM expresses surrogate models as a linear combination of radial basis functions $\psi(r)$ that pass through all sampling points, $x_i \in R^n, i = 1, \ldots, m$, and was defined by [25] as

$$\tilde{F}(x) = \sum_{i=1}^{m} w_i \psi(r_i), \quad (10)$$

where, w_i are the weights of the radial basis functions (RBFs). Each constituent basis function is defined in terms of the Euclidean distance (r_i) between the prediction point $\boldsymbol{x}$ and the ith of basis function center $x_c^{(i)}$, and is expressed as

$$r_i = \left\| x_i - x_c^{(i)} \right\| \quad (11)$$

[24] has divided RBFs into two categories, i.e., non-parametric basis function (Eq. 12, Eq. 13, and Eq. 14) and parametric basis functions (Eq. 15, Eq. 16, and Eq. 17). The following expressions are RBFs.

i. $\psi(r) = r$, - Linear (12)

ii. $\psi(r) = r^3$, - Cubic (13)

iii. $\psi(r) = r^2 \ln r$, - Thin plate spline (14)

iv. $\psi(r) = e^{\frac{-r^2}{(2\sigma^2)}}$, - Gaussian (15)

v. $\psi(r) = (r^2 + \sigma^2)^{1/2}$, and - Multi-quadric (16)

vi. $\psi(r) = (r^2 + \sigma^2)^{-1/2}$. - Inverse multi-quadric (17)

The weights, w_i, are evaluated using all the sampling points x_i and their corresponding function values $\tilde{F}(x)$. Gram matrix $\boldsymbol{\psi}$ is used to represent the matrix of the basis function values at the sampling points [25], and specified as

$$\boldsymbol{\psi} = \begin{bmatrix} \psi(\|x_1 - x_c^{(1)}\|) & \psi(\|x_1 - x_c^{(2)}\|) & \cdots & \psi(\|x_1 - x_c^{(m)}\|) \\ \psi(\|x_2 - x_c^{(1)}\|) & \psi(\|x_2 - x_c^{(2)}\|) & \cdots & \psi(\|x_2 - x_c^{(m)}\|) \\ \vdots & \vdots & \ddots & \vdots \\ \psi(\|x_m - x_c^{(1)}\|) & \psi(\|x_m - x_c^{(2)}\|) & \cdots & \psi(\|x_m - x_c^{(m)}\|) \end{bmatrix} \quad (18)$$

The column vector $\boldsymbol{w}$ is the weights for each radial basis function.

$$\boldsymbol{w} = \begin{Bmatrix} w_1 \\ w_2 \\ \vdots \\ w_m \end{Bmatrix} \quad (19)$$

The column vector $\widetilde{\boldsymbol{F}}$ is the function values of all sampling points ($\tilde{F}(x_1)$).

$$\widetilde{\boldsymbol{F}} = \begin{Bmatrix} \tilde{F}(x_1) \\ \tilde{F}(x_2) \\ \vdots \\ \tilde{F}(x_3) \end{Bmatrix} \quad (20)$$

Similar to polynomial model, w is determined through Moose-Penrose pseudo-inverse of $\boldsymbol{\psi}^+$

$$\boldsymbol{w} = \boldsymbol{\psi}^+ \widetilde{\boldsymbol{F}} \quad (21)$$

Even though Eq. 21 is linear in terms of the basis function weights $\boldsymbol{w}$, but RBFM can representing highly non-linear outputs.

Kriging Model. Matheron in 1963 had introduced the term *Krigeage* which now called as *Kriging*, as appreciation to the method developed by a South African mining engineer, D.G. Krige [25]. Kriging Model is an approach to approximate irregular data. This model consists of two components: (i) a "basis" function, and (ii) Gaussian random function with zero mean. The "basis" function is generally a polynomial (e.g., linear, quadratic, etc.) [1]. The general form of the Kriging model is written as

$$F(\boldsymbol{x}) = f(\boldsymbol{x}) + Z(\boldsymbol{x}) \quad (22)$$

where $Z(\boldsymbol{x})$ is a Gaussian random function with zero mean on the sample space and $f(\boldsymbol{x})$ is a known approximation function which is usually any polynomial functions. Mathematically, $f(\boldsymbol{x})$ is written as

$$f(x) = \sum_{i=1}^{k} \beta_i g_i(x), \quad (23)$$

or, in vector form,

$$f(x) = \boldsymbol{g}^T\boldsymbol{\beta}, \quad (24)$$

where $\boldsymbol{\beta} = [\beta_1, \cdots, \beta_k]$ and $\boldsymbol{g} = [g_k(\boldsymbol{x}), \cdots, g_k(\boldsymbol{x})]^T$.

The covariance matrix of $Z(x)$ is stated as

$$Cov\left[Z\left(\boldsymbol{x}^{(i)}\right), Z\left(\boldsymbol{x}^{(j)}\right)\right] = \sigma^2\boldsymbol{R}\left(R\left(\boldsymbol{x}^{(i)}, \boldsymbol{x}^{(j)}\right)\right), \quad (25)$$

$$i = 1, \cdots, N, j = 1, \cdots, N_{exp}$$

where $x^{(i)}$ and $x^{(j)}$ are two arbitrary points in the sample space, σ^2 is the variance of $Z(\mathrm{x})$, $R\left(\boldsymbol{x}^{(i)}, \boldsymbol{x}^{(j)}\right)$ is the spatial correlation function and $\boldsymbol{R}$ is correlation matrix (Toropov, 2001). A common $\boldsymbol{R}$ expression used is the Gaussian correlation function of the form

$$R\left(\boldsymbol{x}^{(i)}, \boldsymbol{x}^{(j)}\right) = \exp\left[-\sum_{k=1}^{N}\theta_k\left|\boldsymbol{x}_k^{(i)} - \boldsymbol{x}_k^{(j)}\right|^2\right]. \quad (26)$$

The surrogate model is

$$S(\boldsymbol{x}) = \boldsymbol{g}^T(\boldsymbol{x})\boldsymbol{\beta_e} + \boldsymbol{r}^T(\boldsymbol{x})\boldsymbol{R}^{-1}(\boldsymbol{F_s} - \boldsymbol{F\beta_e}), \quad (27)$$

where F_s is an observed responses vector and $\boldsymbol{r}$ is the correlations vector between the response at random location x and sample points. $\boldsymbol{r}$ is written as

$$\boldsymbol{r}(\boldsymbol{x}) = \left\{R\left(\boldsymbol{x}, \boldsymbol{x}^{(1)}\right), \cdots, R\left(\boldsymbol{x}, \boldsymbol{x}^{(N_{exp})}\right)\right\}. \quad (28)$$

It was found that the Radial Basis Function model and Kriging model are mostly used for approximating high-fidelity model's responses. On the other hand, Polynomial model is commonly-known used for developing response surface of actual experiment.

METHODOLOGY

1.1 The Architecture of Vehicle Suspension System Model

Before developing the surrogate model, two models are constructed which are called as low-fidelity (LF) model and high-fidelity (HF) model respectively in this research. LF and HF models are two models to represent a quarter vehicle size and a full vehicle size respectively. Moreover, HF model is more detailed model than the LF model. Many researchers had claimed that the HF model provides better performance prediction than LF model. However, LF are still being used and popular especially because of its simplicity, easy to setup, and portrays quick response review especially for early design stage. The architecture of these models is described in Sub-Section 1.1.1 and Sub-Section 1.1.2.

1.1.1 Low-Fidelity Model

A model for representing a single station of suspension system is called as quarter vehicle model (QVM) as shown in Figure 2. The upper body mass is consisting of the car body and the suspension mass, which is called sprung mass, M_s. The lower mass is the weight of the tire and its axle, called as the unsprung mass, M_u.

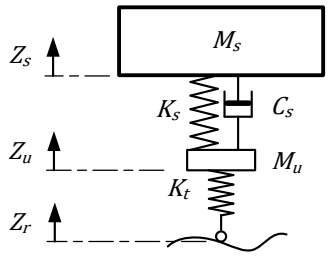

Figure 2: Free-body diagram of QVM or 2-DoF model.

The equations of motion for the QVM [26] are formulated from Newton's second law as

$$M_u\ddot{Z}_u = K_t(Z_r - Z_u) - K_s(Z_u - Z_s) - C_s(\dot{Z}_u - \dot{Z}_s), \quad (29)$$

$$M_s\ddot{Z}_s = K_s(Z_u - Z_s) + C_s(\dot{Z}_u - \dot{Z}_s). \quad (30)$$

1.1.2 High-Fidelity Model

The basis of the high-fidelity model architecture is consisting of four QVMs (as in Figure 3) to represent each vehicle's suspension corner. Then, these four QVMs are coupled with one rigid body that can vertically translate, roll, and pitch about their respective axis at the vehicle's centre of gravity. This model is also known as seven-degrees-of-freedoms lumped mass model. The model is formulated on the basis of three Newton's laws.

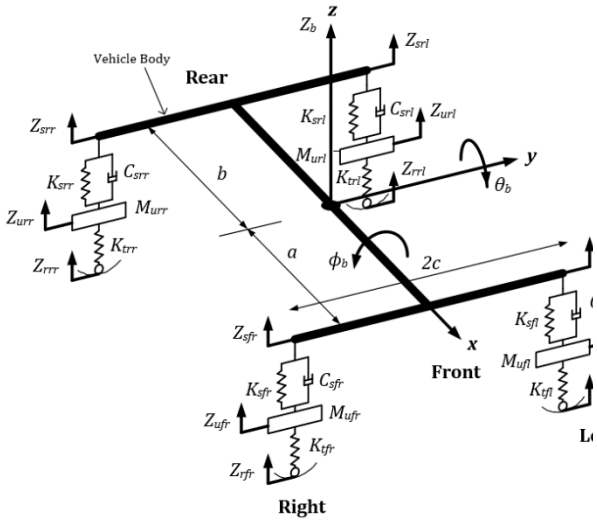

Figure 3: A lumped mass model of vehicle.

Equations of 31 to 34 are vertical translation of unsprung mass for each corner.

$$\ddot{Z}_{ufr} = \frac{K_{tfr}}{M_{ufr}}(Z_{rfr} - Z_{ufr}) - \frac{K_{sfr}}{M_{ufr}}(Z_{ufr} - Z_{sfr}) - \frac{C_{sfr}}{M_{ufr}}(\dot{Z}_{ufr} - \dot{Z}_{sfr}) \quad (31)$$

$$\ddot{Z}_{ufl} = \frac{K_{tfl}}{M_{ufl}}(Z_{rfl} - Z_{ufl}) - \frac{K_{sfl}}{M_{ufl}}(Z_{ufl} - Z_{sfl}) - \frac{C_{sfl}}{M_{ufl}}(\dot{Z}_{ufl} - \dot{Z}_{sfl}) \quad (32)$$

$$\ddot{Z}_{urr} = \frac{K_{trr}}{M_{urr}}(Z_{rrr} - Z_{urr}) - \frac{K_{srr}}{M_{urr}}(Z_{urr} - Z_{srr}) - \frac{C_{srr}}{M_{urr}}(\dot{Z}_{urr} - \dot{Z}_{srr}) \quad (33)$$

$$\ddot{Z}_{url} = \frac{K_{trl}}{M_{url}}(Z_{rrl} - Z_{url}) - \frac{K_{srl}}{M_{url}}(Z_{url} - Z_{srl}) - \frac{C_{srl}}{M_{url}}(\dot{Z}_{url} - \dot{Z}_{srl}) \quad (34)$$

Next three equations of 35, 36, and 37 are description of body motion at the centre of gravity of vehicle in z-axis ($\ddot{Z}_b$), rotation about y-axis ($\ddot{\phi}_b$), and rotation about x-axis ($\ddot{\theta}_b$) as shown in Figure 3.

$$\begin{aligned}\ddot{Z}_b &= \frac{K_{sfr}}{M_b}(Z_{ufr} - Z_{sfr}) + \frac{C_{sfr}}{M_b}(\dot{Z}_{ufr} - \dot{Z}_{sfr}) \\ &+ \frac{K_{sfl}}{M_b}(Z_{ufl} - Z_{sfl}) + \frac{C_{sfl}}{M_b}(\dot{Z}_{ufl} - \dot{Z}_{sfl}) \\ &+ \frac{K_{srr}}{M_b}(Z_{urr} - Z_{srr}) + \frac{C_{srr}}{M_b}(\dot{Z}_{urr} - \dot{Z}_{srr}) \\ &+ \frac{K_{srl}}{M_b}(Z_{url} - Z_{srl}) + \frac{C_{srl}}{M_b}(\dot{Z}_{url} - \dot{Z}_{srl}).\end{aligned} \quad (35)$$

$$\ddot{\phi}_b = -\frac{cK_{sfr}}{I_{xx}}(Z_{ufr} - Z_{sfr}) - \frac{cC_{sfr}}{I_{xx}}(\dot{Z}_{ufr} - \dot{Z}_{sfr}) + \frac{cK_{sfl}}{I_{xx}}(Z_{ufl} - Z_{sfl}) + \frac{cC_{sfl}}{I_{xx}}(\dot{Z}_{ufl} - \dot{Z}_{sfl}) - \frac{cK_{srr}}{I_{xx}}(Z_{urr} - Z_{srr}) - \frac{cC_{srr}}{I_{xx}}(\dot{Z}_{urr} - \dot{Z}_{srr}) + \frac{cK_{srl}}{I_{xx}}(Z_{url} - Z_{srl}) + \frac{cC_{srl}}{I_{xx}}(\dot{Z}_{url} - \dot{Z}_{srl}). \quad (36)$$

$$\ddot{\theta}_b = -\frac{aK_{sfr}}{I_{yy}}(Z_{ufr} - Z_{sfr}) - \frac{aC_{sfr}}{I_{yy}}(\dot{Z}_{ufr} - \dot{Z}_{sfr}) - \frac{aK_{sfl}}{I_{yy}}(Z_{ufl} - Z_{sfl}) - \frac{aC_{sfl}}{I_{yy}}(\dot{Z}_{ufl} - \dot{Z}_{sfl}) + \frac{bK_{srr}}{I_{yy}}(Z_{urr} - Z_{srr}) + \frac{bC_{srr}}{I_{yy}}(\dot{Z}_{urr} - \dot{Z}_{srr}) + \frac{bK_{srl}}{I_{yy}}(Z_{url} - Z_{srl}) + \frac{bC_{srl}}{I_{yy}}(\dot{Z}_{url} - \dot{Z}_{srl}) \quad (37)$$

The following four equations are used to connect four QVM with the vehicle body.

$$\ddot{Z}_{sfr} = \ddot{Z}_b - a\ddot{\theta}_b - c\ddot{\phi}_b \quad (38)$$

$$\ddot{Z}_{sfl} = \ddot{Z}_b - a\ddot{\theta}_b + c\ddot{\phi}_b \quad (39)$$

$$\ddot{Z}_{srr} = \ddot{Z}_b + b\ddot{\theta}_b - c\ddot{\phi}_b \quad (40)$$

$$\ddot{Z}_{srl} = \ddot{Z}_b + b\ddot{\theta}_b + c\ddot{\phi}_b \quad (41)$$

1.2 Vehicle Suspension System Parameters

The vehicle type used for this project is a sedan passenger car with a curb weight of 1270 kg. For a simulation of a quarter vehicle model, the front-end weight is 317.5 kg. Other vehicle data are revealed in Table 1. The data of spring stiffness coefficient and damping coefficient are within a range for a standard passenger car.

1.3 Suspension System Design Boundary

Spring stiffness, K_s and damper rate, C_s are two suspension elements that play an importance role in ride dynamics performance. Several researchers skilled in this vehicle dynamics such as [12], [27], [26], and [4] have proposed three criteria to be used in evaluating the suspension system performance. The three criteria are Suspension Working Space (SWS), Body Acceleration (BAcc), and Dynamic Tyre Load (DTL). According to [28], the design of suspension system is controlled by a few numbers that have not changed since the time of Olley and they will remain forever. The numbers are called as magic number by [28]. [29], [11], and [30] have indicated that all of them agreed on the statement issued by [28]. Therefore, the spring stiffness and damper rate limits can be established as revealed in Table 2.

Table 1: Parameters for full vehicle model.

Parameters	Value
Sprung Mass, M_s	317.5 kg
Unsprung Mass, M_u	45.4 kg
Tire Stiffness, K_t	192 kN/m

Parameters	Value
Moment of inertia about x-axis, I_{xx}	220.45 kgm^2
Moment of inertia about y-axis, I_{yy}	1067.22 kgm^2
Moment of inertia about y-axis, I_{zz}	1181.08 kgm^2
Length of the front wheelbase, a	0.961 m
Length of the rear wheelbase, b	1.504 m
Length of the suspension hard-point to the center line, c	0.723 m
Height of the center of gravity from the roll center, h	0.382 m

Table 2: Operating range of spring stiffness and damper rate of sedan passenger car.

Suspension Elements	Operating Range
Spring Stiffness	12,536 N/m $< K_s <$ 24,570 N/m
Damping Rate	798 Ns/m $< C_s <$ 2235 Ns/m

1.4 The Architecture of Surrogate Model

The rudimentary architecture of the surrogate model, $\tilde{S}(\boldsymbol{x}, \boldsymbol{a})$ is consisting of low-fidelity model's response, $\tilde{f}(\boldsymbol{x})$, high-fidelity model's response, $\tilde{F}(\boldsymbol{x})$, and the tuning coefficients, $\boldsymbol{a}$. The architecture of the surrogate model is mathematically written as

$$\tilde{S}(\boldsymbol{x}, \boldsymbol{a}) \equiv \tilde{F}\left(\tilde{f}(\boldsymbol{x}), \boldsymbol{a}\right) \approx \tilde{F}(\boldsymbol{x}) \tag{42}$$

In this paper, three routines of surrogate model have been formulated which are called as Response Based Model (RBM), Variable Based Model (VBM), Parameter Based Model (PBM).

1.4.1 Response-Based (RB) Model

This model is the first type of surrogate model, $\tilde{S}(\boldsymbol{x}, \boldsymbol{a})$ has a remodel function of linear (Eq. 43) form and is written respectively as

$$\tilde{S}(\boldsymbol{x}, \boldsymbol{a}) = a_0 + a_1 \tilde{f}(\boldsymbol{x}), \tag{43}$$

1.4.2 Variable-Based (VB) Model

In the second type model, the tuning coefficients, $\boldsymbol{a}$ are attached to the design variables and become a tuning function, $t(\boldsymbol{x}, \boldsymbol{a})$. The formulation of the remodel function is expressed as

$$\tilde{S}(\boldsymbol{x}, \boldsymbol{a}) = \tilde{f}(\boldsymbol{x}) + t(\boldsymbol{x}, \boldsymbol{a}), \quad t(\boldsymbol{x}, \boldsymbol{a}) = a_0 + \sum_{i=1}^{N} x_i a_i, \tag{44}$$

Both equations, Eq. 43 and Eq. 44 are intrinsically non-linear model.

1.4.3 Parameter-Based (PB) Model

This routine uses any physical parameters in the low- and high- fidelity models as the tuning coefficient, $\boldsymbol{a}$. This research selects sprung mass as the tuning coefficient. The main reason of introducing this model is to investigate its performance as a surrogate model for the suspension system design. This model is mathematically stated as

$$\tilde{S}(\boldsymbol{x}, \boldsymbol{a}) \equiv \tilde{f}(\boldsymbol{x}, \boldsymbol{a}) \,. \tag{45}$$

1.5 Searching the Optimal Tuning Coefficients

The optimal tuning coefficients for the surrogate model of RBM and VBM is searched by minimizing the sum of the squares of deviation, d between the surrogate model and the high-fidelity model. This searching is an optimization problem. Mathematically, the objective function is stated as

$$\text{Minimize:} \quad d = \sum_{i=1}^{n} \left(\tilde{S}(\boldsymbol{x}, \boldsymbol{a})_i - \tilde{F}(\boldsymbol{x})_i\right)^2 \tag{46}$$

where, n is the number of sampling points and i the sampling point number. Any optimization

methods can be used to search the optimal solution of Eq. 46 [23].

1.6 Accuracy Evaluation of The Surrogate Model

Depending on a single statistical metric such as R-squared are not enough and often lead to misinterpretation of model accuracy evaluation [31]. [32], [33] and [34] in their works had employed three statistical metrics, which are R-Squared (R^2), Root Mean Squared Error ($RMSE$), and Maximum Absolute Error (MAE) to evaluate the accuracy of the surrogate model. $RMSE$ and MAE measure the global response accuracy and the local response accuracy of the model, respectively. Meanwhile, R-Squared indicates the intimacy metric between the surrogate model and the high-fidelity model. The formulas of R^2, MAE, and $RMSE$ are defined as

$$R^2 = 1 - \frac{\sum_{i=1}^{n}\left(\tilde{S}(\boldsymbol{x},\boldsymbol{a})_i - \tilde{F}(\boldsymbol{x})_i\right)^2}{\sum_{i=1}^{n}\left(\bar{F}(\boldsymbol{x}) - \tilde{F}(\boldsymbol{x})_i\right)^2}, \quad (47)$$

$$MAE = \max_{i=1,\dots,n}\left|\tilde{S}(\boldsymbol{x},\boldsymbol{a})_i - \tilde{F}(\boldsymbol{x})_i\right|, \quad \text{and} \quad (48)$$

$$RMSE = \sqrt{\frac{1}{n}\sum_{i=1}^{n}\left(\tilde{S}(\boldsymbol{x},\boldsymbol{a})_i - \tilde{F}(\boldsymbol{x})_i\right.} \quad (49)$$

where, $\bar{F}(x)$ is the average value of the high-fidelity model response. The lowest MAE and RMSE values but highest in R-Squared value indicate the best tuning results for the surrogate model.

RESULTS AND DISCUSSION

The architecture of LF model, HF model, and surrogate models had been constructed in such a way all simulations can take place using the same platform which in this case is in Matlab/Simulink. Each model had run for 400 sampling nodes simulations. As mentioned in Section 5, BAcc, DTL and SWS were three criteria for suspension system design assessment. In this paper, there were three surrogate models have been formulated which were called as RB, VB, and PB model. The final performance results for each surrogate model were reported through the medium of graph figures and tabular statistical data. Table 3 and Figure 4, Table 4 and Figure 5, and Table 5 and Figure 6 show three pair results for surrogate model of RB, VB, and PB models compared to LF and HF models.

Through Figure 4 to Figure 6, it can be visualized that the responses produced by LF model (grey surface) had dissimilar trend compared to HF model (light grey surface) particularly in terms of their respective magnitudes. The orientation of each respective response surfaces was also different between these two models. This show that LF model and HF model have different capability. In fact, these substantial differences have inspired the author to conduct this research. This research is an investigation to find out the feasibility of the LF model to be tuned so as to achieve equivalent output as the HF model. The tuned LF model is called as surrogate model.

Table 3 and Figure 4 are a pair of result for assessing the surrogate model's performance of the RB model. The statistical measure results, the MAE and RMSE, and the R^2 values show close to the best values of 0 (zero) and 1 (one) respectively for all the suspension design criteria, i.e., BAcc, DTL, and SWS. These indicate that the difference between RB model and HF model had a very low-level variance. Furthermore, the graphical results in Figure 4 were found to agree also with those results in Table 3. All the surface responses of BAcc, DTL, and SWS for surrogate model had very close trend to HF model. This simply put the RB model as a useful surrogate model.

The second surrogate model in this feasibility study is VB model. Table 4 reveals the statistical summary of VB model's performance. The summary indicates that all suspension system criteria have almost 100% match to HF model. This can be also visually observed from Figure 5. Similarly, VB model is also a useful surrogate model.

Sprung mass, M_s is used as the tuning coefficient in the PB model. By inspecting Figure 6 and Table 5, the PB model capable to generate equivalent response for BAcc only. The initial sprung mass, M_s of 317.5 kg is reduced to 195.4 kg in order to yield higher BAcc of LF model. Furthermore, PB model has also failed to capture the HF responses for SWS and DTL. It was found that this surrogate model type cannot be trusted since it will easily provide incorrect interpretation of real behaviour of the suspension system.

Table 3: The accuracy performance of RB model

		KEY PERFORMANCE INDICATORS		
		BAcc	DTL	SWS
Assessment Criteria	MAE	0.0879	4.1415×10^{-3}	3.4127×10^{-4}
	RMSE	0.0351	2.2850×10^{-3}	1.7969×10^{-4}
	R^2	0.9218	0.9970	0.9526
Tuning Parameters	a_0	-0.1774	109.4078	0.0010
	a_1	1.8149	0.7473	0.9999

CONCLUSION

This research has introducing three approaches in deriving surrogate model. The models are called as RB model, VB model, and PB model. Among these three models, the PB model is the most unreliable model. The main flaw on PB model is the changing of parameter could lead to unrealistic behaviour of suspension system in even though the gap between surrogate model and HF model is close as indicated in Figure 6. MAE, RMSE, and R^2 were three key performance indicators (KPIs) used in evaluating the variance performance of surrogate model relative to HF model. Based on KPIs values and graph visualisation, the RB and VB models were considered as two useful surrogate models. Moreover, the VB model gave slightly more satisfy as surrogate model than the RB model. As a conclusion, the attempt to conduct a feasibility study of surrogate model for vehicle suspension system has successfully achieved.

ACKNOWLEDGEMENTS

The authors would like to thank Professor Dr Vassili Toropov and Professor Dr Martin Levesley from Leeds University, England for guiding me at the beginning of this research.

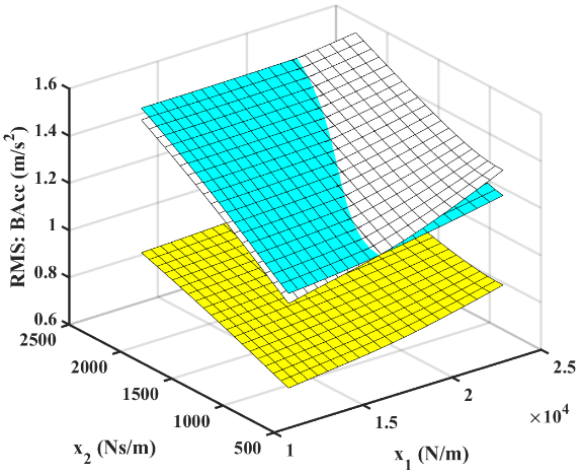

(a)

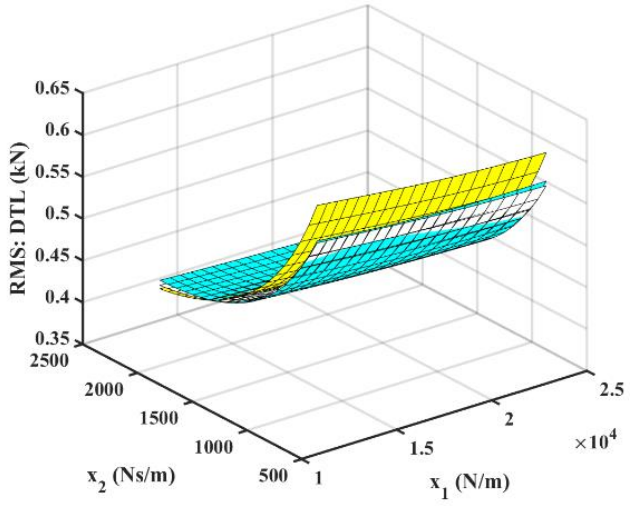

(b)

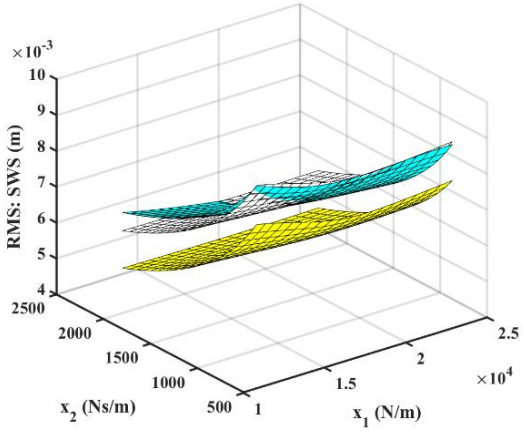

(c)

Figure 4: RB model's responses of (a) BAcc, (b) DTL, and (c) SWS. All diagrams have three surfaces. Yellow surface is low-fidelity model's response, cyan surface is high-fidelity model's response, and white surface is surrogate model's response.

Table 4: The accuracy performance of VB model

		KEY PERFORMANCE INDICATORS		
		BAcc	DTL	SWS
Assessment Criteria	MAE	0.0064	7.8310 × 10^{-3}	1.5637 × 10^{-4}
	RMSE	0.0026	2.9671 × 10^{-3}	7.1046 × 10^{-5}
	R^2	0.9996	0.9950	0.9926
Tuning Parameters	a_0	0.3251	-61.1685	0.0019
	a_1	-2.7149e-06	1.8652e-04	-4.5169e-08
	a_2	1.4559e-04	0.0322	5.0812e-09

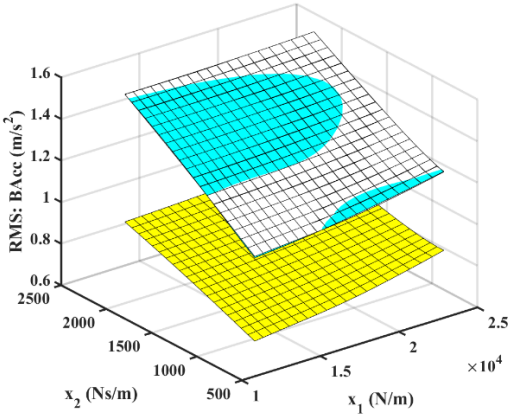

(a)

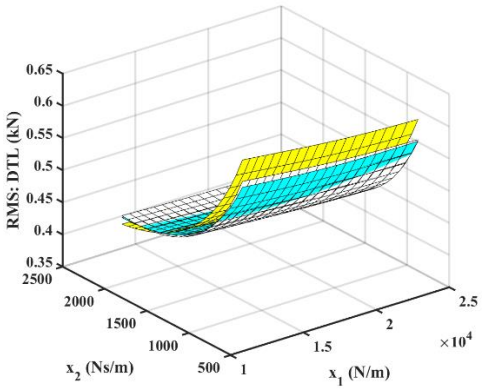

(b)

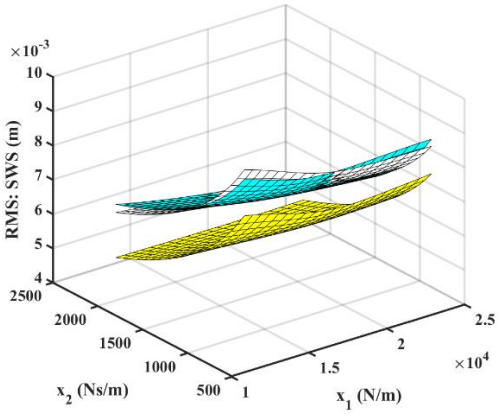

(c)

Figure 5: VB model's responses of (a) BAcc, (b) DTL, and (c) SWS. All diagrams have three surfaces. Yellow surface is low-fidelity model's response, cyan surface is high-fidelity model's response, and white surface is surrogate model's response.

Table 5: The accuracy performance of PB model

		KEY PERFORMANCE INDICATORS		
		BAcc	DTL	SWS
Assessment Criteria	MAE	0.0731	38.5780 × 10^{-3}	7.5847 × 10^{-4}
	RMSE	0.0295	16.7876 × 10^{-3}	3.0715 × 10^{-4}
	R^2	0.9475	0.8476	0.8684
Tuning Parameters	M_s (kg)	195.4	263.3	451.6

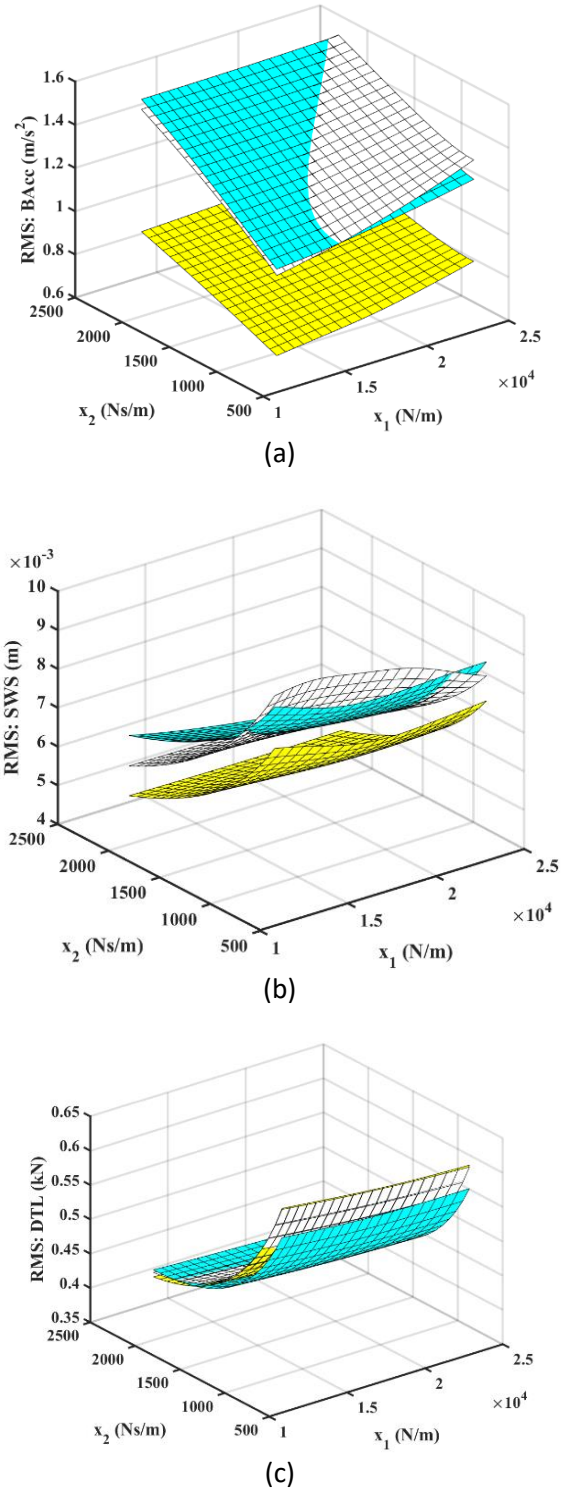

Figure 6: PB model's responses of (a) BAcc, (b) DTL, and (c) SWS. Yellow surface is low-fidelity model's response, cyan surface is high-fidelity model's response, and white surface is surrogate model's response.

Nomenclature

C_s	damping rate (Ns/m)
C_{sfr}	damping rate for front right end (Ns/m)
C_{sfl}	damping rate for front left end (Ns/m)
C_{srr}	damping rate for rear right end (Ns/m)
C_{srl}	damping rate for rear left end (Ns/m)
K_s	spring stiffness (N/m)
K_{sfr}	spring stiffness for front right end (N/m)
K_{sfl}	spring stiffness for front left end (N/m)
K_{srr}	spring stiffness for rear right end (N/m)
K_{srl}	spring stiffness for rear left end (N/m)
K_t	tire stiffness (N/m)
K_{tfr}	tire stiffness for front right end (N/m)
K_{tfl}	tire stiffness for front left end (N/m)
K_{trr}	tire stiffness for rear right end (N/m)
K_{trl}	tire stiffness for rear left end (N/m)
M_s	sprung mass (kg)
M_b	body mass (kg)
M_u	unsprung mass (kg)
M_{ufr}	unsprung mass for front right end (kg)
M_{ufl}	unsprung mass for front left end (kg)
M_{urr}	unsprung mass for rear right end (kg)
M_{url}	unsprung mass for rear left end (kg)
Z_b	body displacement (m)
Z_r	road displacement (m)
Z_{rfr}	road displacement at front right end (m)
Z_{rfl}	road displacement at front left end (m)
Z_{rrr}	road displacement at rear right end (m)
Z_{rrl}	road displacement at rear left end (m)
Z_s	sprung displacement (m)
Z_{sfr}	sprung displacement at front right end (m)
Z_{sfl}	sprung displacement at front left end (m)
Z_{srr}	sprung displacement at rear right end (m)
Z_{srl}	sprung displacement at rear left end (m)
Z_u	unsprung displacement (m)
Z_{ufr}	unsprung displacement at front right end (m)
Z_{ufl}	unsprung displacement at front left end (m)
Z_{urr}	unsprung displacement at rear right end (m)
Z_{url}	unsprung displacement at rear left end (m)
θ_b	rolling angle (rad)
ϕ	pitching angle (rad)

REFERENCES

[1] *Papalambros, P.Y., and Wilde, W.J., 2017. Principles of Optimal Design: Modeling and Computation, 3rd. Edition. Cambridge University Press.*

[2] *Kiencke, U. and Nielsen, L., 2000. Automotive Control Systems: For Engine, Driveline, and Vehicle. Germany, Springer Berlin-Heidelberg.*

[3] *Koziel, S., and Leifsson, L., 2013. In Koziel, S., and Leifsson, L. (Eds). Surrogate-Based Modeling and Optimization: Applications in Engineering. Springer New York Heidelberg Dordrecht London.*

[4] *Blundell, M. and Harty, D., 2015. The Multibody Systems Approach to Vehicle Dynamics. 2nd. Edition. United Kingdom. Elsevier Butterworth-Heinemann.*

[5] *Sharp, R.S., 1991. Computer Codes for Road Vehicle Dynamic Models. Institution of Mechanical Engineers Paper 427/16/064, Autotech '91, Birmingham.*

[6] *Uys, P.E., Els, P.S., and Thoresson, M.J., 2006. Criteria for Handling Measurement. Journal of Terramechanics 43. 43-67.*

[7] Gobbi, M., Haque, I., Papalambros P.P.Y., and Mastinu, G., 2006. A Critical Review of Optimization Methods for Road Vehicles Design, 11th AIAA/ISSMO Multi-Disciplinary Analysis and Optimization Conference. 6 - 8 September 2006. Portsmouth, Virginia: American Institute of Aeronautics and Astronautics, Inc.

[8] Berci, M., Toropov, V.V., Hewson, R.W., and Gaskell, P.H., 2009. Metamodeling Based on High and Low Fidelity Models Interaction for UAV Gust Performance Optimization. 50th AAIA/ASME/ASCE.AHS/ASC Structures, Structural Dynamics, and Materials conference. 4-7 May. California, Palm Springs, 1-40.

[9] Bhosekar, A. and Ierapetritou, M., 2018. Advances in Surrogate-based Modeling, Feasibility Analysis, and Optimization: A Review. Computers & Chemical Engineering. An International Journal of Computer Applications in Chemical Engineering. Volume 108. pp 250-256.

[10] Storey, I., Bourmistrova, A., and Subic, A. (2008). Performance Measures of Comfort and Rattlespace Usage for Limited-Stroke Vehicle Suspension Systems. International Journal of Acoustics and Vibrations. Vol. 13(2), pp. 1-9.

[11] Dukkipati, R., Pang, J., Qatu, M.S., Sheng, G., and Shuguang, Z., 2008. Road Vehicle Dynamics. Warrendale PA: SAE International.

[12] Olley, M., 1946. Road Manners of the Modern Car. Proceedings of the Institution of Automobile Engineers. September, Vol. 41, 523-551.

[13] Jazar, R.N., 2017. Vehicle Dynamics: Theory and Application. Third Edition. Springer International Publishing.

[14] Sun, T., Zhang, Y., and Barak, P., 2002. 4-DOF Vehicle Ride Model, SAE Technical Series. 2002-01-1580.

[15] Kim, C., and Ro, P.I., 2002. An Accurate Full Car Ride Model Using Model Reducing Techniques. Journal of Mechanical Design. Transactions of the ASME. Vol. 124, pp. 697 – 705.

[16] Firth, G.R., 1991. The Performance of Vehicle Suspensions Fitted With Controllable Dampers. PhD Thesis, The University of Leeds, Leeds.

[17] Hyvarinen, J.K., 2004. The Improvement of Full Vehicle Semi-Active Suspension Through Kinematical Model. PhD Thesis. University of Oulu.

[18] Ghike, C., and Shim, T., 2006. 14 Degree-of-Freedom Vehicle Model for Roll Dynamics Study. SAE Technical Paper Series. 2006-01-1277.

[19] Samin, P.M., 2010. Hybrid Stability Augmentation System-Force Control of Semi-Active Suspension with Magnetorheological Damper. PhD Thesis. Universiti Teknologi Malaysia, Skudai.

[20] Chapra, S., 2018. Applied Numerical Methods with MATLAB for Engineers and Scientists. Fourth Edition. NewYork: McGraw-Hill Education.

[21] Gilat, A. and Subramaniam, V., 2013. Numerical Methods for Engineers and Scientists. Third Edition. Wiley Global Education.

[22] Toropov, V.V., Van Keulen, F., Markine, V.L., Alvarez, L.F., 1999. Multipoint Approximations Based on Response Surface Fitting: A Summary of Recent Developments. Proceedings of the 1st ASMO UK/ISSMO Conference, Ilkley, pp. 371–380. Bradford: MCB University Press.

[23] Toropov, V.V., 2001. Modeling and Approximation Strategies in Optimization: Global and Mid-Range Approximation, Response Surface Methods, Genetic Programming, Low / High Fidelity Models. In Balchut, J. and Eschenauer, H.A. (Eds). Emerging Methods for Multidisciplinary Optimization, 205-256. Italy: Springer-Verlag Wien New York.

[24] Messac, A. (2015). Optimization in Practice with MATLAB for Engineering Students and Professionals. United States of America: Cambridge University Press.

[25] Forrester, A.I.J., Sobester, A., and Keane, A.J., 2008. Engineering Design via Surrogate Modelling: A Practical Guide. UK: John Wiley & Sons. Ltd.

[26] Crolla, D.A., 1995. Vehicle Dynamics - Theory into Practice. Automobile Division Chairman's Address, Institution of Mechanical Engineers.

[27] Gilliespie, T. D., 1992. Fundamentals of Vehicle Dynamics. USA: SAE Publications.

[28] Barak, P., 1991. Magic Numbers in Design of Suspension for Passenger Car. SAE Technical Paper Series. 911921, pp. 53-88.

[29] Nunney, M.J., 2007. Light and Heavy Vehicle Technology. 4th Edition. Butterworth-Heinemann.

[30] Popp, K., and Schiehlen, W., 2010. Ground Vehicle Dynamics. Germany: Springer-Verlag Berlin Heidelberg.

[31] Chapra, S.C. and Canale, R.P., 2020. Numerical Methods for Engineers. 8th Edition. New York. Mc Graw Hill.

[32] Wang, G.G., and Shan, S., 2006. Review of Metamodeling Techniques in Support of Engineering Design Optimization. ASME 2006 International Design Engineering Technical Conferences and Computers and Information in Engineering Conference. Volume 1: 32nd Design Automation Conference, Parts A and B.

[33] Jiang, R., Jin, Z., Liu, D., and Wang, D., 2021. Multi-Objective Lightweight Optimization of Parameterized Suspension Components Based on NSGA-II Algorithm Coupling with Surrogate Model. Machines 2021, 9, 107.

[34] Fouladinejad, N., Fouladinejad, Jalil, M.K.A, and Taib, J.M., 2017. Decomposition-Assisted Computational Technique Based on Surrogate Modeling for Real-Time Simulations. Complexity. Vol. 2017. Article ID 1686230.